APS physics

CHORUS

This is the accepted manuscript made available via CHORUS. The article has been published as:

Quantized Single-Ion-Channel Hodgkin-Huxley Model for Quantum Neurons

Tasio Gonzalez-Raya, Xiao-Hang Cheng, Iñigo L. Egusquiza, Xi Chen, Mikel Sanz, and Enrique Solano

Phys. Rev. Applied **12**, 014037 — Published 22 July 2019

DOI: 10.1103/PhysRevApplied.12.014037

Quantized Single Ion Channel Hodgkin-Huxley Model for Quantum Neurons

Tasio Gonzalez-Raya,[1] Xiao-Hang Cheng,[2] Iñigo L. Egusquiza,[3] Xi Chen,[1,4] Mikel Sanz,[1,*] and Enrique Solano[1,4,5]

[1] *Department of Physical Chemistry, University of the Basque Country UPV/EHU, Apartado 644, 48080 Bilbao, Spain*
[2] *Department of Physics, Shanghai University, 200444 Shanghai, China*
[3] *Department of Theoretical Physics and History of Science, University of the Basque Country UPV/EHU, Apartado 644, 48080 Bilbao, Spain*
[4] *International Center of Quantum Artificial Intelligence for Science and Technology (QuArtist) and Department of Physics, Shanghai University, 200444 Shanghai, China*
[5] *IKERBASQUE, Basque Foundation for Science, Maria Diaz de Haro 3, 48013 Bilbao, Spain*

The Hodgkin-Huxley model describes the behavior of the cell membrane in neurons, treating each part of it as an electric circuit element, namely capacitors, memristors, and voltage sources. We focus on the activation channel of potassium ions, due to its simplicity, while keeping most of the features displayed by the original model. This reduced version is essentially a classical memristor, a resistor whose resistance depends on the history of electric signals that have crossed it, coupled to a voltage source and a capacitor. Here, we will consider a quantized Hodgkin-Huxley model based on a quantum memristor formalism. We compare the behavior of the membrane voltage and the potassium channel conductance, when the circuit is subjected to AC sources, in both classical and quantum realms. Numerical simulations show an expected adaptation of the considered channel conductance depending on the signal history in all regimes. Remarkably, the computation of higher moments of the voltage manifest purely quantum features related to the circuit zero-point energy. Finally, we study the implementation of the Hodgkin-Huxley quantum memristor as an asymmetric rf SQUID in superconducting circuits. This study may allow the construction of quantum neuron networks inspired in the brain function, as well as the design of neuromorphic quantum architectures for quantum machine learning.

I. INTRODUCTION

Brain science and neurophysiology are fascinating topics posing deep questions regarding the global comprehension of the human being. Understanding how the brain works catalyzed interdisciplinary research fields such as biophysics and bioinformatics. In 1963, the Nobel Prize in Physiology or Medicine was awarded to Alan Lloyd Hodgkin and Andrew Fielding Huxley for their work describing how electric signals in neurons propagate through the axon. This work consists on modeling small segments of the axon membrane as an electric circuit represented by a set of non-linear differential equations [1–4], establishing a bridge between neuroscience [5, 6] and physics [7–14].

A neuron is an electrically excitable cell that receives, processes, and transmits information through electric signals, whose main components are the cell body, the dendrites, and the axon. Dendrites are ramifications which receive and transmit stimuli into the cell body, which processes the signal. The nerve impulse is then propagated through the axon, which is an extension of the nerve cell. This propagation gradient is generated through the change in the ion permeability of the cell membrane when an impulse is transmitted. This implies a variation in ion concentrations represented in the Hodgkin-Huxley circuit by a non-linear conductance. Its resistance depends on the history of electric charges crossing the cell, which is naturally identified with a memristor [16, 17].

In the last decade, we have witnessed a blossoming of quantum platforms for quantum technologies, where quantum simulations, quantum computing, quantum sensing, and quantum communication are to be highlighted. Superconducting circuits is one of the leading quantum platforms, allowing for controllability, scalability, and coherence. The combination of biosciences with quantum technologies gave rise to a variety of novel fields, as quantum artificial intelligence [18], quantum biology [19, 20], quantum artificial life [21, 22], and quantum biomimetics [23], among others. From a wide perspective, we are heading towards a general framework for neuromorphic quantum computing, in which brain-inspired architectures strive to take advantage of quantum features to enhance computational power.

Recent proposals for a quantized memristor [24], as well as its possible implementations in both superconducting circuits [25] and integrated quantum photonics [26], allows for the construction of a quantized neuron model based on Hodgkin-Huxley circuit. In the classical realm, this model reproduces the characteristic adaptive behavior of brain neurons. Whereas, in the quantum regime, it could unveil unique characteristics or an unprecedented learning performance. Furthermore, the study of memristor-based electric circuits [27–30] sets a starting position for the investigation of coupled quantum memristors, which may lead to the development of quantum neuron networks.

Classical models comprising features of real neurons is an active research field, leaving open an extension to the quantum domain [31–36]. This lead to the prolongation of neuromorphic computing towards the quantum

* mikel.sanz@ehu.eus

realm. Neuromorphic quantum computing consists in the design of artificial structures that mimic neurobiological architectures present in the nervous system with the purpose of enhancing and accelerating certain computational tasks, utilizing quantum resources [37]. Furthermore, classical memristive devices have been used in the simulation of synaptic [38–40] as well as learning processes [41]. However, none of those works ever considered the quantized version of the Hodgkin-Huxley model.

In this article, we study a simplified version of the Hodgkin-Huxley model, preserving its biological interest, in which only the potassium ion channel plays a role. The ion channel conductance, modelled by a memristor, is coupled to a voltage source and a capacitor, where we study its response under a periodic driving in both classical and quantum regimes. By means of a quantum memristor [24], we quantize the elements of the considered Hodgkin-Huxley circuit, comparing the membrane voltage, the conductance, and the I-V characteristic curve for a classical input source [42]. To conclude, we look into the implementation of the quantum memristor in the Hodgkin-Huxley circuit as an asymmetric rf SQUID in superconducting circuits. This work establishes a roadmap for the experimental construction of quantum neuron networks, as well as neuromorphic quantum architectures and quantum neural networks [43]. These concepts could find general applications in the field of quantum machine learning [44] and a challenging alternative to a gate-based universal quantum computer.

II. THEORETICAL FRAMEWORK

A. Classical Hodgkin-Huxley model

The cell membrane of a neuron shows permeability changes for different ion species after receiving electric impulses through the dendrites. These changes result in variations on ion concentrations which, when a certain threshold is overcome, can lead to a sudden depolarization of the membrane and the consequent transmission of the signal through the axon. These ions comprise mainly potassium and sodium, which have different roles during a potential spike. In 1952, Hodgkin and Huxley developed a model which describes the propagation of these stimuli by treating each component of the excitable cell membrane as an electric circuit element, as shown in Fig. 1(a). The equations of this circuit are

$$I(t) = C_g \frac{dV_g}{dt} + \bar{g}_K n^4 (V_g - V_K) + \bar{g}_{N_a} m^3 h (V_g - V_{N_a}) + \bar{g}_L (V_g - V_L), \quad (1)$$

$$\frac{dn}{dt} = \alpha_n(V_g)(1-n) - \beta_n(V_g) n, \quad (2)$$

$$\frac{dm}{dt} = \alpha_m(V_g)(1-m) - \beta_m(V_g) m, \quad (3)$$

$$\frac{dh}{dt} = \alpha_h(V_g)(1-h) - \beta_h(V_g) h, \quad (4)$$

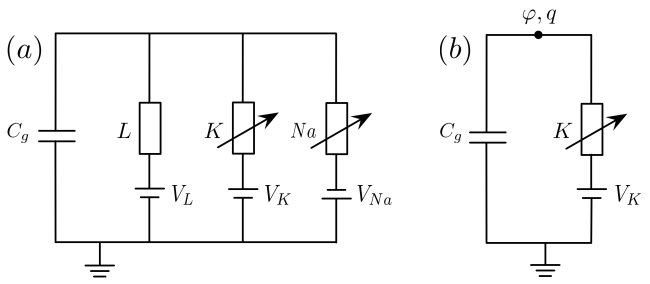

FIG. 1. (a) Complete Hodgkin-Huxley circuit and (b) Hodgkin-Huxley circuit with solely a potassium ion channel. The capacitance C_g describes the axon's membrane capacity to store charge, the voltage sources V_i account for the initial ion concentrations in the axon, and the ion permeabilities of the membrane are described by non-linear conductances i, for $i = L, K, Na$.

where I is the total current, $\bar{g}_i$ $(i = L, K, N_a)$ are constants representing the maximum value each electrical conductance can take. C_g is the membrane capacitance, V_i is the resting potential in each ion channel, and n, m, and h are dimensionless quantities between 0 and 1 that represent the probability of activation or inactivation of each ion channel.

Except for the leakage channel L, which accounts for small unperturbed flow of non-involved (mostly chloride) ions, and thus is described by a constant conductance, any ion channel is characterized by a non-linear conductance due to n, m and h, which weigh each channel differently and depend on voltage and time. Here, we keep solely the contribution coming from the potassium channel, which only has activation gates, and not both activation and inactivation gates as the sodium channel. This model still conserves the most characteristic behavior of neurons. In this case, we are left with two coupled differential equations,

$$I(t) = C_g \frac{dV_g}{dt} + g_K n^4 (V_g - V_K), \quad (5)$$

$$\frac{dn}{dt} = \alpha_n(V_g)(1-n) - \beta_n(V_g) n. \quad (6)$$

Naturally, this non-linear conductance can be identified with a memristor.

B. Memristor

The memristor is a resistor whose resistance depends on the history of electrical signals, voltages or charges, that have crossed it. This particular description of a resistor can be given in the context of Kubo's response theory [15], and it was in 1971 when L. O. Chua rescued this idea and coined the term "memristor" [16]. In the original work by A. L. Hodgkin and A. F. Huxley, the memristor does not appear as an independent electric circuit element, but as a nonlinear resistor governed by

the equations of a memristor. This identification came about years later, and is highlighted in Ref. [45]. The equations describing the physical properties and memory effects of a (voltage-controlled) memristor are

$$I(t) = G(\mu(t))V(t), \tag{7}$$
$$\dot{\mu}(t) = f(\mu(t), V(t)). \tag{8}$$

$G(\cdot)$ and $f(\cdot)$ are continuous real functions satisfying

(i) $G(\mu) \geq 0$ for all values of μ.

(ii) For a fixed μ, $f(\mu, V)$ is monotone, and $f(\mu, 0) = 0$.

Property (i) implies that $G(\mu)$ can indeed be understood as a conductance, so that Eq. (7) can be interpreted as a state-dependent Ohm's law. This ensures that the memristor is a passive element. Property (ii) restricts the internal variable dynamics to provide non-vanishing memory effects for all significant voltage inputs, implying that it does not have dynamics in the absence of voltage.

Notice that solving Eq. (8) requires time integration over the past of the control signal, and this solution affects $G(\mu)$. This means that the response in the current given by Eq. (7) depends not only on the present value of the control voltage, but also on the previous ones. Hence, if a memristor undergoes a periodic control signal, the I-V characteristic curve will display a hysteresis loop, which contains memory effects, identifying the slope of this curve with the resistance of the device.

The study of a single ion channel means neutralizing the dynamics of the other channel, which is a matter of controlling its voltage, namely its ionic concentration. Experimentally, an isolated study of the potassium channel is achieved by setting the membrane voltage to V_{Na}, or through changing the sodium concentration by replacing the sodic medium by any other non-gated substance. This was performed in Ref. [4], and allowed them to obtain experimental results that could be compared to theoretical ones, thus testing the proposed expressions for α_x and β_x, with $x = n, m, h$ separately for each channel, so that values for n, m, h could be obtained. Then, with the conductance of the potassium channel given by $g_K = \bar{g}_K n^4$, Eqs. 5 and 6 can be solved numerically for the membrane voltage, given an input current $I(t)$.

C. Circuit Quantization

Now we give a brief introduction to circuit quantization. To do so, we first describe the quantization of the memristor. The quantum memristor has been recently introduced [24], and is described as a non-linear element in a closed circuit with a weak-measurement scheme, used to update the resistance. This layout can be seen in Fig. 2(a) as a closed system coupled to a resistor and a measurement apparatus, introducing a measurement-based update of the resistance depending on the system voltage.

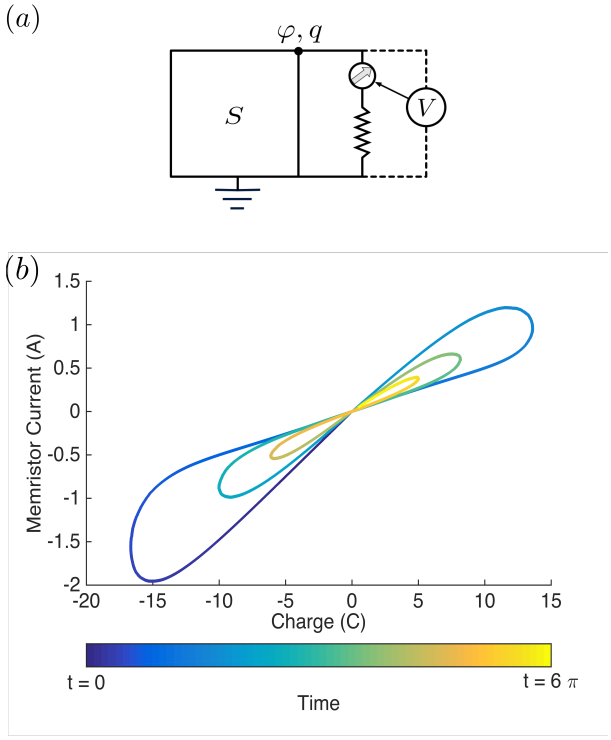

FIG. 2. (a) Diagram of a quantum memristor as a resistor coupled to a closed system with a voltage-based weak-measurement scheme. (b) Hysteresis loops displayed by a quantum memristor coupled to a LC circuit with a system Hamiltonian $H_S = \frac{q^2}{2C} + \frac{\varphi^2}{2L}$, with $C = 1$F and $L = 1$H. The memristor current is measured in C/s, and the charge in C. Time is defined as the inverse of the frequency, through 3 full cycles of the memristive device.

The dynamics of the composite system can be studied by a master equation composed of Hamiltonian, continuous-weak-measurement, and dissipation parts,

$$d\rho = d\rho_H + d\rho_m + d\rho_d. \tag{9}$$

The Hamiltonian part is given by von Neumann equation,

$$d\rho_H = -\frac{i}{\hbar}[H_S, \rho(t)]dt. \tag{10}$$

The continuous-weak-measurement part reads

$$d\rho_m = -\frac{\tau}{q_0^2}[q, [q, \rho(t)]]dt + \sqrt{\frac{2\tau}{q_0^2}}(\{q, \rho(t)\} - 2\langle q\rangle\rho(t))dW, \tag{11}$$

where $[\cdot, \cdot]$ denotes a commutator and $\{\cdot, \cdot\}$ an anticommutator. The expectation value of an observable is $\langle A\rangle = \mathrm{tr}(\rho A)$, τ is the projection frequency, q_0 is the uncertainty, the measurement strength is defined as $\kappa = \frac{\tau}{q_0^2}$, and dW is the Wiener increment, related to the stochasticity associated with weak measurements.

The dissipation is described by a Caldeira-Leggett

master equation,

$$d\rho_d = -\frac{i\gamma(\mu)}{\hbar}[\varphi,\{q,\rho(t)\}]dt - \frac{2C\lambda\gamma(\mu)}{\hbar}[\varphi,[\varphi,\rho(t)]]dt, \tag{12}$$

where $\lambda = k_B T/\hbar$ and $\gamma(\mu)$ is the relaxation rate. Solving these equations, we can have the relation between memristive current and the charge shown in Fig. 2(b), for an LC circuit coupled to a memristor, with a Hamiltonian of the form $H_S = \frac{q^2}{2C} + \frac{\varphi^2}{2L}$. We can observe the memristor displays the characteristic hysteresis curve when plotting the current response versus the charge, which is related to the control voltage as $V = q/C$. In the case of a circuit with classical sources, or a circuit coupled to an open element, there is no need to introduce the Wiener noise.

With a Hamiltonian formulation on sight, a description of electric circuits entails defining fluxes and charges, from which the voltage and the current can be obtained by time differentiation. In this case we employ a node formulation, where node fluxes are the main variables and play the role of the spatial variable, with node charges being the conjugate variables. This formulation with node fluxes suffices to describe a circuit featuring linear capacitances and inductances.

In a Lagrangian formalism, dissipative elements such as resistors can be treated by adding a dissipation function to the equations of motion of an effective Lagrangian [46]. However, the reversibility of Hamilton's equations, arising from a Hamiltonian formulation needed for a proper circuit quantization, conflicts with the irreversibility of dissipative terms. To describe the quantum memristor in a Lagrangian formulation suitable for canonical quantization, we assume linear dissipation and treat it as a linear dissipative element in the Caldeira-Leggett model [47]. In this manner, we replace it by an infinite set of coupled LC oscillators with a frequency-dependent impedance $Z(\omega)$, i.e. a transmission line. We identify the impedance of the transmission line with the resistance of the memristor and, assuming that the time between consecutive updates is much larger than the memristor's relaxation time, the impedance can be updated (see Fig. 3).

III. QUANTIZED HODGKIN-HUXLEY MODEL

A. Classical input source

We now study the quantization of the Hodgkin-Huxley circuit in Fig. 3. For this, we write the Lagrangian describing this circuit,

$$\begin{aligned}\mathcal{L} =& \frac{C_g}{2}(\dot\phi_0 - \dot\phi_s)^2 + \frac{C_c}{2}\dot\phi_0^2 - \frac{(\phi_1-\phi_0)^2}{2\Delta x L_0} + \\ &+ \sum_{i=1}^{\infty}\left[\frac{\Delta x C_0}{2}(\dot\phi_i - V_0)^2 - \frac{(\phi_{i+1}-\phi_i)^2}{2\Delta x L_0}\right].\end{aligned} \tag{13}$$

C_0 and L_0 are the characteristic capacitance and impedance per unit length of the transmission line, and

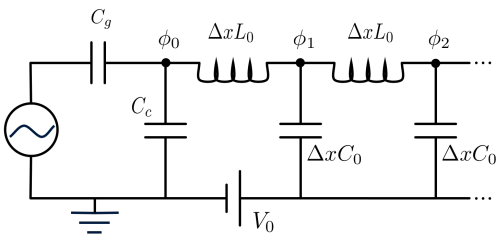

FIG. 3. Hodgkin-Huxley circuit for a single ion channel with a classical AC source, $I(t) = I_0\sin(\Omega t)$, coupled to a semi-infinite transmission line. C_0 and L_0 are the capacitance and inductance corresponding to the transmission line, C_g is the capacitance coupling the source to the circuit, C_c accounts for the axon's membrane capacitance, and V_0 is the resting potential for the potassium ion channel.

the classical current source is defined as $I(t) = -C_g(\ddot\phi_0 - \ddot\phi_s)$. The motion of this circuit can be described by Euler-Lagrange equations, $\frac{\mathrm{d}}{\mathrm{d}t}\frac{\partial\mathcal{L}}{\partial\dot\phi} = \frac{\partial\mathcal{L}}{\partial\phi}$. Computing these equations for the intermediate node fluxes on the transmission line, ϕ_i, we find

$$\ddot\phi_i = \frac{1}{L_0 C_0}\frac{\partial^2\phi_i}{\partial x^2} \tag{14}$$

after taking the continuum limit, $\Delta x \to 0$. This is the wave equation for a flux field at position x_i on the transmission line. The general solution to this equation can be written in terms of ingoing and outgoing waves, $\phi(x,t) = \phi_{\mathrm{in}}(t + x/v) + \phi_{\mathrm{out}}(t - x/v)$, with velocity $v = 1/\sqrt{L_0 C_0}$. This leads to the relations

$$\begin{aligned}\frac{\partial\phi(x,t)}{\partial t} &= \dot\phi_{\mathrm{in}}(t+x/v) + \dot\phi_{\mathrm{out}}(t-x/v),\\ \frac{\partial\phi(x,t)}{\partial x} &= \frac{1}{v}(\dot\phi_{\mathrm{in}}(t+x/v) - \dot\phi_{\mathrm{out}}(t-x/v)),\end{aligned} \tag{15}$$

which allows us to obtain $\frac{\partial\phi_0(t)}{\partial x} = \frac{1}{v}(2\dot\phi_{\mathrm{in}}(t) - \dot\phi_0(t))$. The Euler-Lagrange equation for ϕ_0 is

$$-I(t) + C_c\ddot\phi_0 = \frac{1}{L_0}\frac{\partial\phi_0}{\partial x} \tag{16}$$

having taken the continuum limit. We can rewrite this as

$$-I(t) + C_c\ddot\phi_0 + \frac{\dot\phi_0}{Z_0} = 2\frac{\dot\phi_0^{\mathrm{in}}}{Z_0}, \tag{17}$$

where $Z_0 = \sqrt{L_0/C_0}$ is the impedance of the transmission line, associated with the resistance of the memristor. $\phi_0(t)$ is our main variable because $\langle\dot\phi_0(t)\rangle$ will give us the circuit voltage, for a given state of the transmission line. We have identified $\phi_0(t)$ with $\phi(x=0,t)$, the flux field inside the transmission line at $x = 0$, and we want then to quantize this flux.

Given that the wave equation inside the transmission line is satisfied, the flux field can be written in terms of ingoing and outgoing modes, fulfilling canonical commutation relations for a semi-infinite transmission line. This sets the starting point for the quantization of the field, which has been performed for infinite electrical networks, see Ref. [48]. To begin, we write the decomposition

$$\begin{aligned}\phi(x,t) =&\sqrt{\frac{\hbar Z_0}{4\pi}}\int_0^\infty \frac{d\omega}{\sqrt{\omega}}(a_{in}(\omega)e^{i(k_\omega x-\omega t)}+\\ &+a_{out}(\omega)e^{-i(k_\omega x+\omega t)}+\text{H.c.}),\end{aligned} \tag{18}$$

where $k_\omega = |\omega|\sqrt{L_0C_0}$ is the wave vector. Here, $a_{\text{in}}(\omega)$ and $a_{\text{out}}(\omega)$ can be promoted to quantum operators, and thus $\phi_0(t)$ is promoted to a quantum operator. By combining Eq. (17) with Eq. (18) and writing the Fourier transform of the current, $I(t) = \int_0^\infty \frac{d\omega}{\sqrt{\omega}}(\mathcal{I}(\omega)e^{-i\omega t} + \mathcal{I}^*(\omega)e^{i\omega t})$, we can express the outgoing modes in terms of the ingoing ones,

$$a_{\text{out}}(\omega) = a_{\text{in}}(\omega)\frac{i-C_c\omega Z_0}{i+C_c\omega Z_0} - \frac{1}{\omega}\sqrt{\frac{4\pi Z_0}{\hbar}}\frac{\mathcal{I}(\omega)}{i+C_c\omega Z_0}. \tag{19}$$

$R(\omega) = \frac{i-C_c\omega Z_0}{i+C_c\omega Z_0}$ is the reflection coefficient, and we identify $s(\omega) = \frac{1}{\omega}\sqrt{\frac{4\pi Z_0}{\hbar}}\frac{\mathcal{I}(\omega)}{i+C_c\omega Z_0}$ as the source term, with $\mathcal{I}(\omega) = \frac{\sqrt{\omega}}{2\pi}\int_{-\infty}^{\infty} dt e^{i\omega t}I(t)$. Then the circuit voltage is

$$\begin{aligned}\langle\dot{\phi}_0(t)\rangle = &-i\sqrt{\frac{\hbar Z_0}{4\pi}}\int_0^\infty d\omega\sqrt{\omega}\\ &\Big[\Big(\langle a_{\text{in}}(\omega)\rangle(1+R(\omega)) - s(\omega)\Big)e^{-i\omega t} - \text{H.c.}\Big]\end{aligned} \tag{20}$$

for a given state of the transmission line. By choosing this state to be the vaccum, $\langle 0|a_{\text{in}}(\omega)|0\rangle = \langle 0|a^\dagger_{\text{in}}(\omega)|0\rangle = 0$, and for a classical input current $I(t) = I_0\sin(\Omega t)$, the voltage response of the system reads

$$\langle\dot{\phi}_0\rangle = I_0Z_0\frac{\sin(\Omega t) - C_c\Omega Z_0\cos(\Omega t)}{1+(C_c\Omega Z_0)^2}. \tag{21}$$

Actually, this is what is obtained when studying the stationary solution of Eq. (17) with $\dot{\phi}_0^{\text{in}} = 0$. However, we claim that ϕ_0 is a valid quantum operator, and to demonstrate this we compute the second moment of the voltage. We do this for a vaccum state of the transmission line, meaning no excitations, and find

$$\begin{aligned}\langle\dot{\phi}_0^2\rangle =&\frac{\hbar Z_0}{\pi}\int_0^\infty d\omega\,\frac{\omega}{1+(C_c\omega Z_0)^2} +\\ &+\Big[Z_0I_0\frac{\sin(\Omega t) - C_c\Omega Z_0\cos(\Omega t)}{1+(C_c\Omega Z_0)^2}\Big]^2.\end{aligned} \tag{22}$$

The second term contains the voltage squared, which has a classical origin, at variance with the first term. The latter is related to the reflection of the modes in the circuit and is associated with the zero-point energy. It diverges as $\omega\to\infty$, which is a purely quantum mechanical effect [47]. We can eliminate the divergence in the voltage fluctuations by subtracting this quantity to the second moment of the voltage computed for the transmission line in a thermal state. This state is defined through Bose-Einstein statistics,

$$\begin{aligned}&\langle a_{\text{in}}(\omega)a_{\text{in}}(\omega')\rangle = \langle a^\dagger_{\text{in}}(\omega)a^\dagger_{\text{in}}(\omega')\rangle = 0,\\ &\langle a^\dagger_{\text{in}}(\omega)a_{\text{in}}(\omega')\rangle = \frac{1}{2}\Big[\coth\big(\frac{\beta\hbar\omega}{2}\big)-1\Big]\delta(\omega-\omega'),\\ &\langle a_{\text{in}}(\omega)a^\dagger_{\text{in}}(\omega')\rangle = \frac{1}{2}\Big[\coth\big(\frac{\beta\hbar\omega}{2}\big)+1\Big]\delta(\omega-\omega'),\end{aligned} \tag{23}$$

for the number of bosonic modes. Here, $\beta = 1/k_BT$, k_B is the Boltzmann constant and T is the temperature. Then, we need to compute the following integral

$$\begin{aligned}&\Delta \equiv \langle\dot{\phi}_0^2\rangle_{\text{Thermal}} - \langle\dot{\phi}_0^2\rangle_{\text{Vacuum}} =\\ &\frac{\hbar Z_0}{\pi}\int_0^\infty d\omega\frac{\omega}{1+(C_c\omega Z_0)^2}\Big[\coth\big(\frac{\beta\hbar\omega}{2}\big)-1\Big],\end{aligned} \tag{24}$$

which by imposing $\hbar\beta\omega \gg 1$ reduces to

$$\frac{2\hbar Z_0}{\pi}\int_0^\infty d\omega\frac{\omega\, e^{-\beta\hbar\omega}}{1+(C_c\omega Z_0)^2} \tag{25}$$

Approximating the solution for large β up to second order, we find

$$\Delta = \frac{2Z_0}{\hbar\pi\beta^2}. \tag{26}$$

This gives the contribution of the quantum fluctuations of the circuit voltage without the zero-point energy. As expected, this quantity goes to cero as $T\to 0$.

In order to observe the system memristive behavior, we introduce the update of the resistance of the memristor, considering the dependence of Z_0 on the circuit voltage. This approach is valid as long as the relaxation time of the set of LC oscillators, which represents the instantaneous resistor, is much shorter than the time scale associated to the change in the resistance. This is equivalent to an adiabatic approximation [49], where we initially consider Z_0 as constant to obtain the value of the circuit voltage and is consistently updated later.

Identifying the inverse of the impedance (known as admittance) with a conductance, we can use the potassium channel conductance $g_K(t) = \bar{g}_K n(t)^4$ to update the impedance $Z(t) = Z_{\min}n(t)^{-4}$, via Eq. (6), such that

$$\dot{Z}(t) = -4Z_{\min}\Big(\frac{Z(t)}{Z_{\min}}\Big)^{5/4}\alpha(V_g) + 4Z(t)\Big(\alpha(V_g)+\beta(V_g)\Big). \tag{27}$$

Thus, from now on, we identify the potassium channel conductance with the inverse of the impedance of the transmission line. Notice that, in this treatment, we have assumed that the voltage measurements used to update the impedance of the memristor do not perturbe the system, considering measurements in this setup to be automatic and non-invasive. Given the dependence of the

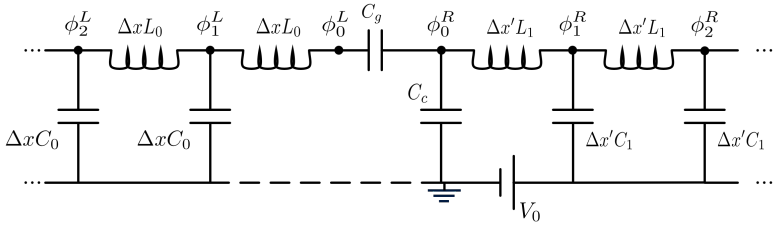

FIG. 4. Hodgkin-Huxley circuit for a single ion channel coupled to a semi-infinite transmission line, introducing a quantized source on the left modelled by a second semi-infinite transmission line. C_0 and L_0 are the capacitance and inductance corresponding to the left transmission line, and the ones corresponding to the right transmission line are C_1 and L_1. C_g is the capacitance coupling both transmission lines, C_c accounts for the axon's membrane capacitance, and V_0 is the resting potential for the potassium ion channel.

impedance on the circuit voltage, we solve Eq. (27) numerically to obtain the change in impedance of the memristor. Then, we compute the potassium channel conductance and the membrane voltage. This is equivalent, as mentioned above, to a strong adiabatic approximation, in which the impedance is considered constant in order to update the voltage of the circuit.

B. Quantized input source

To study the circuit response to quantum state inputs, we replace the source with a second semi-infinite transmission line, thus introducing a collection of LC circuits in which multiple frequencies can be excited. This circuit is depicted in Fig. 4. In this scenario, the input current will be introduced by $\langle \dot{Q}_0^L \rangle$, where $Q_0^L = C_g(\dot{\phi}_0^L - \dot{\phi}_0^R)$, for a given state that satisfies $\langle \dot{Q}_0^L \rangle = I_0 \sin(\Omega t)$. The Lagrangian describing this system is

$$\begin{aligned}\mathcal{L} = &\sum_{i=1}^{\infty}\left[\frac{\Delta x C_0}{2}(\dot{\phi}_i^L)^2 - \frac{(\phi_i^L - \phi_{i+1}^L)^2}{2\Delta x L_0}\right] - \frac{(\phi_0^L - \phi_1^L)^2}{2\Delta x L_0} \\ &+ \frac{C_g}{2}(\dot{\phi}_0^R - \dot{\phi}_0^L)^2 + \frac{C_c}{2}(\dot{\phi}_0^R)^2 - \frac{(\phi_1^R - \phi_0^R)^2}{2\Delta x' L_1} \\ &+ \sum_{j=1}^{\infty}\left[\frac{\Delta x' C_1}{2}(\dot{\phi}_j^R - V_0)^2 - \frac{(\phi_{j+1}^R - \phi_j^R)^2}{2\Delta x' L_1}\right],\end{aligned} \tag{28}$$

where the capacitance and inductance corresponding to the left transmission line are C_0 and L_0, and the ones corresponding to the right transmission line are C_1 and L_1. The Euler-Lagrange equations for ϕ_0^L and ϕ_0^R are

$$C_g(\ddot{\phi}_0^L - \ddot{\phi}_0^R) = \frac{2\dot{\phi}_{in}^L(t)}{Z_0} - \frac{\dot{\phi}_0^L}{Z_0}, \tag{29}$$

$$C_g(\ddot{\phi}_0^R - \ddot{\phi}_0^L) + C_c\ddot{\phi}_0^R = \frac{2\dot{\phi}_{in}^R(t)}{Z_1} - \frac{\dot{\phi}_0^R}{Z_1}, \tag{30}$$

respectively. Z_0 is the impedance on the left transmission line, and Z_1 the one on the right transmission line. These equations can be written in this manner, since the wave equation is satisfied inside each of the transmission lines for a flux field. We use the Euler-Lagrange equations to find expression for the outgoing modes in terms of the ingoing ones,

$$\begin{aligned}a_{\text{out}}^L(\omega) &= a_{\text{in}}^L(\omega)R_0(\omega) + a_{\text{in}}^R(\omega)s(\omega), \\ a_{\text{out}}^R(\omega) &= a_{\text{in}}^R(\omega)R_1(\omega) + a_{\text{in}}^L(\omega)s(\omega).\end{aligned} \tag{31}$$

Now, these modes have reflected and transmitted contributions on both sides of the circuit. The reflection coefficients are given by

$$\begin{aligned}R_0(\omega) &= \frac{1 - i\omega(C_g + C_c)Z_1 + \omega C_g Z_0(i + \omega C_c Z_1)}{1 - i\omega(C_g + C_c)Z_1 - \omega C_g Z_0(i + \omega C_c Z_1)}, \\ R_1(\omega) &= \frac{1 + i\omega(C_g + C_c)Z_1 - \omega C_g Z_0(i - \omega C_c Z_1)}{1 - i\omega(C_g + C_c)Z_1 - \omega C_g Z_0(i + \omega C_c Z_1)},\end{aligned} \tag{32}$$

and the transmission coefficients by

$$s(\omega) = \frac{-2i\omega C_g\sqrt{Z_0 Z_1}}{1 - i\omega(C_g + C_c)Z_1 - \omega C_g Z_0(i + \omega C_c Z_1)}. \tag{33}$$

Averaging over the vacuum state of the right transmission line, we write the voltage response of the circuit for a given state for the source

$$\langle\dot{\phi}_0^R\rangle = -C_g Z_1\sqrt{\frac{\hbar Z_0}{\pi}}\int_0^\infty d\omega\,\omega^{3/2}\left\{\frac{(1-\omega^2 C_g C_c Z_0 Z_1)\big(\langle a_{\rm in}^L(\omega)\rangle e^{-i\omega t}+\langle a_{\rm in}^{L\dagger}(\omega)\rangle e^{i\omega t}\big)}{1+\omega^2\big(C_g^2Z_0^2+2C_g^2Z_0Z_1+((C_c+C_g)^2+\omega^2C_g^2C_c^2Z_0^2)Z_1^2\big)}\right.$$
$$\left.+\frac{i\omega\big((C_c+C_g)Z_1+C_gZ_0\big)\big(\langle a_{\rm in}^L(\omega)\rangle e^{-i\omega t}-\langle a_{\rm in}^{L\dagger}(\omega)\rangle e^{i\omega t}\big)}{1+\omega^2\big(C_g^2Z_0^2+2C_g^2Z_0Z_1+((C_c+C_g)^2+\omega^2C_g^2C_c^2Z_0^2)Z_1^2\big)}\right\}. \tag{34}$$

Computing the second moment of the voltage, we find

$$\langle(\dot{\phi}_0^R)^2\rangle = \frac{\hbar Z_1}{\pi}\int_0^\infty d\omega\,\frac{\omega(1+\omega^2C_g^2Z_0^2)}{1+\omega^2\big(C_g^2Z_0^2+2C_g^2Z_0Z_1+((C_c+C_g)^2+\omega^2C_g^2C_c^2Z_0^2)Z_1^2\big)}$$
$$-\frac{\hbar Z_1}{4\pi}\int d\omega d\omega'\,\sqrt{\omega\omega'}\Big\{\langle a_{\rm in}^L(\omega)a_{\rm in}^L(\omega')\rangle s(\omega)s(\omega')e^{-i(\omega+\omega')t}-\langle a_{\rm in}^L(\omega)a_{\rm in}^{L\dagger}(\omega')\rangle s(\omega)s^*(\omega')e^{-i(\omega-\omega')t} \tag{35}$$
$$-\langle a_{\rm in}^{L\dagger}(\omega)a_{\rm in}^L(\omega')\rangle s^*(\omega)s(\omega')e^{i(\omega-\omega')t}+\langle a_{\rm in}^{L\dagger}(\omega)a_{\rm in}^{L\dagger}(\omega')\rangle s^*(\omega)s^*(\omega')e^{i(\omega+\omega')t}\Big\},$$

where the first term is again related to the reflection of the modes on the circuit, and it is purely quantum. The second term gives the frequency correlations of the modes on the left transmission line.

The following step would be to find a quantum state of the source which gives the desired input current in the circuit, and to explore what quantum features can be used to enhance this model or to reveal interesting dynamics.

IV. NUMERICAL SIMULATIONS

In this section, we present the results of the membrane voltage and the potassium channel conductance for the single-ion channel Hodgkin-Huxley model. This is done by solving Eq. (27) for the update of the memristor impedance using the results of the membrane voltage. We introduce the solutions of membrane voltage and potassium ion channel conductance for the single-channel Hodgkin-Huxley model, which we use to compare with the results for the quantized Hodgkin-Huxley model with a classical AC current source. In each case, we find that the potassium conductance reproduces qualitatively and approximately the s-shaped curve of Ref. [4].

A. Classical Hodgkin-Huxley model

The single-channel Hodgkin-Huxley model with an AC current source is simulated by solving the Hodgkin-Huxley equations, i.e. Eq. (5) together with Eq. (6). Then, we plot in Fig. 5 the membrane voltage, the potassium channel conductance, and the sodium channel conductance, for a periodic input of the form $I(t) = I_0\sin(\Omega t)$. For the membrane voltage taken to be initially zero, we plot it versus time in Fig. 5(a) as the blue curve, the red curve in Fig. 5(b) corresponding to the potassium channel conductance.

A spike in the membrane voltage can be observed, with a subsequent decrease and adaptation to the input, leading to oscillations around the zero value. This is because we have taken the resting membrane voltage to be zero initially, and have set $V_K = 0$, where normally it is taken to be $V_K = -77$mV. We have chosen this according with the results for the response of the quantized model, in which this classical DC voltage source does not appear. This does not change the dynamical behavior, it just gives a displacement of the voltage. In fact, the profile of the voltage, aside from the oscillations caused by our choice of input current, accurately fits the plots depicted in Ref. [4]. The potassium conductance is reproduced with great accuracy according to Ref. [4], featuring rising and adaptive behavior.

Comparing the conductance as the red curve in Fig. 5(b) with the ones obtained in Ref. [4], it can be appreciated that, with the introduction of an input signal, the conductance rises and adapts to this signal, according to the depolarization of the membrane, with oscillations caused by our choice of $I(t)$. The I-V characteristic curve in Fig. 5(c) displays a hysteresis loop due to the periodic driving, which forms a limit cycle when the system saturates.

It is interesting to see that the spiking behavior of the membrane voltage can be reproduced in this simplified model featuring only potassium conductance. As the values for the coefficients $\alpha(V_g)$ and $\beta(V_g)$ were obtained through comparison with experimental results [4], the gate-opening probabilities for different ion channels may not be completely independent. The, the mechanism of each ion channel cannot be isolated, as the transmission of the nerve impulse is a balanced process involving (in this case, two) different ion permeability changes.

When we solve the quantized Hodgkin-Huxley model, we use an adiabatic approximation. In order to fairly compare the classical and quantized models, we need to study the classical Hodgkin-Huxley model with an adiabatic approximation. The potassium conductance is given by $g_K = \bar{g}_K n^4(t)$. Then, when solving Eqs. (5) and (6), we consider $n(t)$ to be constant. Consequently,

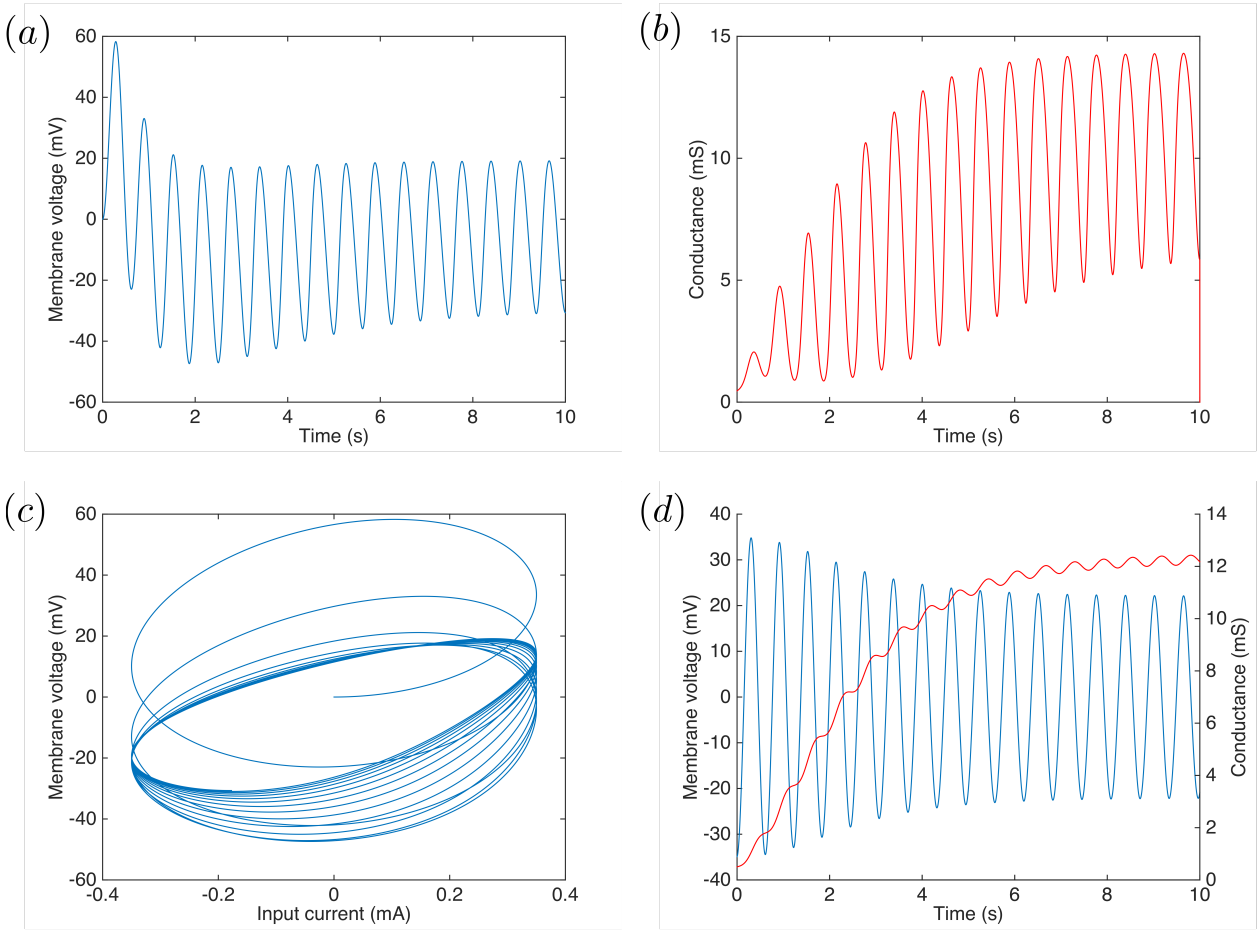

FIG. 5. Classical Hodgkin-Huxley model for a single ion channel with a periodic input $I(t) = I_0 \sin(\Omega t)$: (a) Membrane voltage (blue) over time. (b) Potassium channel conductance (red) over time. (c) Membrane voltage versus input current. (d) Membrane voltage (blue) and potassium channel conductance (red) over time with an adiabatic approximation. The membrane voltage is measured in mV, the input current is in mA, and the potassium channel conductance appears in S.

the straightforward solution of $V_g(t)$ with the choice of input current, $I(t) = I_0 \sin(\Omega t)$, reads

$$V_g(t) = V_K + I_0 \frac{g_K \sin(\Omega t) - \Omega C_g \cos(\Omega t)}{g_K^2 + C_g^2 \Omega^2}. \tag{36}$$

Here, we have only considered the stationary solution, given that the transient one provides fast decay. Using this result, we solve $n(t)$ at any time step. Then, we plot the results of the membrane voltage and the potassium channel conductance as the blue curve and the red curve in Fig. 5(d), respectively. This result is exactly what we obtained in Eq. (21), meaning that the voltage response of the system is classical while the second moment of the voltage displays purely quantum terms.

B. Quantized Hodgkin-Huxley model

The simulation of the quantum Hodgkin-Huxley model uses a classical AC current source. On the other hand, the solutions for the membrane voltage, the potassium channel conductance, and the characteristic I-V curve are presented below. By solving Eqs. (21) and (27), we obtain the membrane voltage and the potassium conductance in the quantum model with a classical input $I(t) = I_0 \sin(\Omega t)$. The membrane voltage against time is plotted as the blue curve in Fig. 6(a). There, we observe a decrease in amplitude and a relaxation of the oscillations as it adapts to the input.

The conductance in Fig. 6(a) (red curve) does not feature a desired delay in its growth, but its saturation is clear, and it resembles the desired s-shaped curve displayed by the saturation of the potassium conductance in Ref. [4]. Note that the membrane voltage and the potassium channel conductance plotted in Fig. 6(a) are the same as in Fig. 5(d), illustrating our statement that the response to a classical input source in the quantum regime is the same as in the classical one with an adiabatic approximation. We introduce the I-V characteristic curve as we plot the membrane voltage versus the input current, shown in Fig. 6(b), featuring a memristive hysteresis loop. The system will have longer saturation

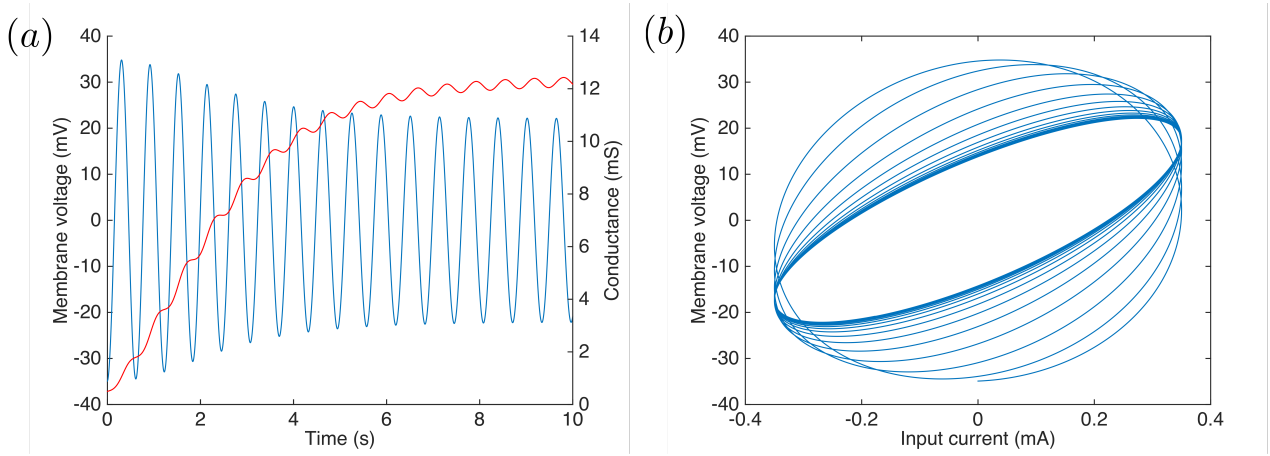

FIG. 6. Quantum Hodgkin-Huxley model for a single ion channel with a classical periodic input $I(t) = I_0 \sin(\Omega t)$: (a) Membrane voltage (blue) and potassium conductance (red) over time. (b) Membrane voltage versus input current. The membrane voltage is measured in mV, the input current is in mA, and the potassium channel conductance appears in S.

times when the initial values are further away from the final value of the impedance. However, the system always relaxes into a limit cycle independent of the initial conditions.

The area of the hysteresis loop can give us a hint about the memory persistence in the system [25, 26], such that the larger the area, the greater the memory persistence. Then, it would be interesting to test whether the introduction of a quantized Hodgkin-Huxley model, allowing for the use of quantum state inputs, represents an improvement in the persistence of the memory. Particularly, entangled states are the desired states for this test. The information carried out by quantum states can be related to classical information through Landauer's principle, being classical dissipation the link, where the area of the hysteresis loop intervenes.

V. FEASIBILITY OF THE IMPLEMENTATION IN SUPERCONDUCTING CIRCUITS

To complete our description of the Hodgkin-Huxley model in the quantum regime, we present a range in which the Hodgkin-Huxley circuit can be implemented in a superconducting platform. For that, we make use of the quantum memristor in superconducting circuits, as presented in Ref. [25]. This model consists of a superconducting loop interrupted by a dc SQUID with negligible loop inductance, and threaded by a bias flux. In this circuit, the dc SQUID behaves as an effective flux-tunable Josephson junction, controlled by the bias flux that threads the superconducting loop. In the latter, critical currents can be suppressed by applying to it a bias flux of half a flux quantum. Furthermore, the two junctions in the dc SQUID are chosen to be from different materials, so that their conductances are different. In the limit of strong conductance asymmetry ($G_1 \gg G_2$), tunneling of quasi-particles is favored ($\Delta_1 \ll \Delta_2$), while critical currents can still be suppressed [50]. This introduces nonlinearities in the circuit by means of a leakage current in the effective junction.

A requirement for this description is that the bias flux is changed adiabatically to avoid the generation of quasiparticles, thus restricting the adiabatic parameter to $\max(\alpha_{\rm rs}) \approx 0.15$ for a sinusoidal driving of the bias flux. Furthermore, this device operates in the low-energy regime, $\hbar\omega_{10}, \delta E \ll 2\Delta$, with a high frequency requirement, $\hbar\omega_{10} \gg \delta E$. Here, $\omega_{10} = \sqrt{2E_C E_L}/\hbar$ is the system transition frequency, being E_C and E_L the capacitive and inductive energies of the junction, respectively. Also, δE is the characteristic energy of quasiparticles above the superconducting gap $\Delta \sim E_L$. The regime in which this implementation would function can be seen in Table I.

The equations of a memristive system can be obtained by means of the conductance of this device, which represents the connection between the quasi-particle (qp) current and the voltage across the total junction, having eliminated the critical currents in the dc SQUID. This way, we obtain a set of equations that mimic those of the clasical memristor introduced in Ref. [50].

$$\langle \hat{I}_{\rm qp} \rangle = G_{\rm qp}[\langle\hat{\varphi}\rangle, \langle\hat{V}\rangle, t]\langle\hat{V}\rangle,$$
$$G_{\rm qp}[\langle\hat{\varphi}\rangle, \langle\hat{V}\rangle, t] = G_0 \sin^2\left[\frac{\pi}{4} + \frac{1}{2}\sin(\omega_{10}t)\right],$$
$$\langle\hat{V}\rangle = V_0 \cos(\omega_{10}t),$$

where

$$G_0 = g_0^2 e^{-g_0^2}\omega_{10}\frac{C_d}{2}\cdot 10^{-4} \approx 3.045\cdot 10^{-9} S,$$
$$g_0 = \left(\frac{E_c}{32E_L}\right)^{1/4} \approx 7.476\cdot 10^{-2},$$

and $\langle\hat{\varphi}\rangle$ is the internal variable of the quantum memristor. In this setting, the dynamics of the internal variable is suppressed in favor of the dynamics of the conductance.

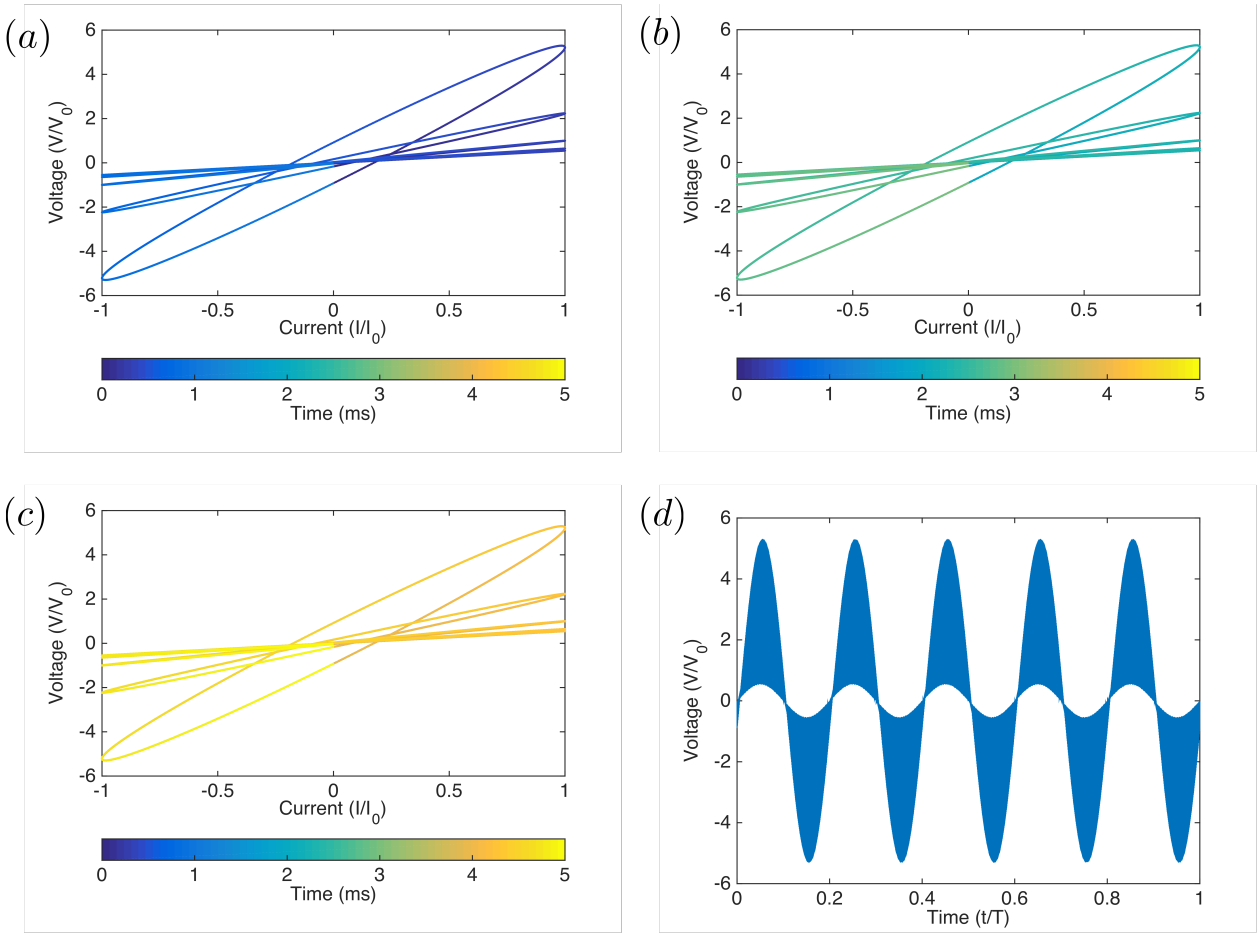

FIG. 7. Numerical simulations of the quantized Hodgkin-Huxley model with a classical current source, introducing a quantum memristor engineered in a superconducting platform. (a) Membrane voltage versus input current for one period of the driving current. (b) Membrane voltage versus input current for three periods of the driving current. (c) Membrane voltage versus input current for the duration of the potential spike. (d) Membrane voltage versus time for the duration of the potential spike (5 ms). The membrane voltage and input current presented here are normalized to V/V_0 and I/I_0, respectively.

E_C	E_L	ω_{10}	Δ	δE	$\alpha_{\rm rs}$
Capacitive energy	Inductive energy	Transition frequency	Superconducting gap energy	Quasiparticle energy	Adiabatic parameter
$2\pi\hbar$ GHz	$10^3 \cdot 2\pi\hbar$ GHz	$44.72 \cdot 2\pi$ GHz	$\sim E_L$	$\ll \hbar\omega_{10}$	≤ 0.15

TABLE I. Numerical values for the regime in which the quantum memristor is implemented in superconducting circuits, taken from Ref. [25].

We then introduce this conductance as the inverse of the impedance in the equation for the membrane voltage in the Hodgkin-Huxley model,

$$\langle \dot{\phi}_0(t) \rangle = V_g(t) = I_0 Z \, \frac{\sin(\Omega t) - C_c \Omega Z \cos(\Omega t)}{1 + C_c^2 \Omega^2 Z^2}. \quad (37)$$

In Table II we give a regime in which the quantum memristor can be implemented in this architecture, and propose a complementary regime in which the behavior of the Hodgkin-Huxley circuit elements can be observed. At the same time, claims about the relaxation time of the memristor and the adiabatic approximation need to be fulfilled. See that this claim is satisfied, as the relaxation time of the memristor is given by $T_{10}(\sim \mu s)$, which is much smaller than the estimated duration of a potential spike, $T_{\rm spike}(\sim 5\, ms)$, in the membrane of the axon. Also, the frequency of the driving is larger than that associated with the period of the spike. With these values, we are able to reproduce the hysteresis loop of the memristor when displaying the membrane voltage versus the input

Architecture	$\omega(2\pi$ Hz)	T(s)	C(F)	G_0 (S)
Superconducting Q. Mem.	$\omega_{10} \sim 4.5 \cdot 10^{10}$	$T_{10} \sim 10^{-6}$	$C_d \sim 5 \cdot 10^{-13}$	$3 \cdot 10^{-9}$
Hodgkin-Huxley model	$\Omega \sim 10^3$	$T_{\text{spike}} \sim 5 \cdot 10^{-3}$	$C_c \sim 10^{-13}$	-

TABLE II. Numerical values for the simulation of the Hodgkin-Huxley circuit with the equations of the quantum memristor engineered in superconducting circuits.

current, as we have $C_c\Omega/\bar{G} \sim 0.0328 \ll 1$ on average, which leads to

$$V(t) \sim \frac{I(t)}{G(t)} = \frac{I_0}{G_0} \frac{\sin(\Omega t)}{\sin^2\left[\frac{\pi}{4} + \frac{1}{2}\sin(\omega_{10} t)\right]} \tag{38}$$

In Fig. 7 we plot the membrane voltage versus the input current (V/V_0 vs I/I_0), displaying multiple hysteresis loops as the system relaxes. In this plot we can observe three different time scales, $T_{10} \sim \mu s$, $T_\Omega \sim ms$, and $T_{\text{spike}} \sim 5\, ms$. We have plotted three different stages of the I-V curve: (a) 1 ms, describing one period of the input current source, (b) 3 ms, describing three periods of the input current source, and (c) 5 ms, describing 5 periods of the input current source, equivalent to the duration of the voltage spike in neurons. In (d) we plot the membrane voltage (V/V_0) versus time, for the duration of the voltage spike. We observe a modulation of the oscillations of the circuit voltage due to the different time scales in this implementation.

The conductance in this case oscillates rapidly. As the internal dynamics of the quantum memristor are supressed, we cannot see the rise of the potassium channel conductance. A solution for this could be to study a model with two parallely connected quantum memristors, but perhaps more effective would be to modify the superconducting qubit that produces memristive behavior. Adding another Josephson junction to the SQUID that interrupts the superconducting loop could add a flux which can be controlled. This way we can compensate for the suppression of the internal variable dynamics.

VI. CONCLUSIONS & PERSPECTIVES

We have studied a simplified version of the Hodgkin-Huxley model with a single ion channel as a circuit featuring a capacitance, a voltage source, and a memristor, both under a periodic input in the classical regime and in the quantum regime. The latter was achieved by introducing the concept of quantum memristor. Then, we compared the membrane voltage, the potassium conductance, and the I-V characteristic curve in both regimes.

This work shows that the behavior of this simplified version of the classical Hodgkin-Huxley model can be reproduced in the quantum regime. The voltage response of the circuit is found to be classical, but the second moment features a quantum mechanical term given by the reflection of the modes in the circuit. The conductance is in good accordance with the experiments carried out in Ref. [4], rising as a s-shaped curve. This is a result of a displacement from a resting value by an input source with an eventual adaptation, unaffected by intermediate and relaxation oscillations. This saturation or adaptation is identified with a learning process by the quantum memristor.

We have also studied the implementation of this circuit in current state-of-the-art quantum technologies, by replacing the ion channel quantum memristor by a superconducting quantum memristor. In this setup, we have found a regime in which the properties of the superconducting quantum memristor can be observed, while the dynamics of the Hodgkin-Huxley circuit remain relevant.

A study of the two-ion channel Hodgkin-Huxley model in the quantum regime amounts to adding a second memristor corresponding to the conductance of the sodium channel [51]. This would unveil new characteristics of the mechanism that rules the conduction of nerve impulses in neurons. Among other things, we would expect to see an initial spike in the sodium conductance, knowing that the mechanism of the sodium channel consists of a fast activation gate followed by inactivation. All this will require an additional effort in the model, a study of two quantum memristors coupled in parallel.

Another interesting line to follow is to study the effects of quantum state inputs on the system, where memory effects are revealed by the area of the hysteresis loop. However, memory effects are more relevant when displayed in connected neuron networks. Studying, for example, the output of a string of neurons with an entangled state input would imply yet another novel discovery: the dynamics of two serially-connected circuits involving quantum memristors. Recent work describing the dynamics of serially and parallelly coupled quantum memristor circuits [27–29] can give an answer to these two questions when taken to a quantum regime. This would set excellent starting points for any advances in neuromorphic quantum computing and quantum neural networks, with direct applications on quantum machine learning.

ACKNOWLEDGMENTS

The authors acknowledge support from Spanish Government PGC2018-095113-B-I00 (MCIU/AEI/FEDER, UE) and Basque Government IT986-16. The authors also acknowledge support from the projects QMiCS (820505)

and OpenSuperQ (820363) of the EU Flagship on Quantum Technologies, as well as the and EU FET Open Grant Quromorphic. This material is also based upon work supported by the U.S. Department of Energy, Office of Science, Office of Advance Scientific Computing Research (ASCR), under field work proposal number ERKJ333.

[1] A. L. Hodgkin and A. F. Huxley, Currents carried by sodium and potassium ions through the membrane of the giant axon of *Loligo*, J. Physiol. **116**, 449 (1952).

[2] A. L. Hodgkin and A. F. Huxley, The components of membrane conductance in the giant axon of *Loligo*, J. Physiol. **116**, 473 (1952).

[3] A. L. Hodgkin and A. F. Huxley, The dual effect of membrane potential on sodium conductance in the giant axon of *Loligo*, J. Physiol. **116**, 497 (1952).

[4] A. L. Hodgkin and A. F. Huxley, A quantitative description of membrane current and its application to conduction and excitation in nerve, J. Physiol. **117**, 500 (1952).

[5] M. I. Rabinovich, P. Varona, A. I. Selverston, H. D. I. Abarbanel, "Dynamical principles in neuroscience", Rev. Mod. Phys. **78**, 1213 (2006).

[6] W. Gerstner, W. M. Kistler, R. Naud, and L. Paninski, *Neuronal Dynamics: From single neurons to networks and models of cognition*, Cambridge University press (2014).

[7] S.-G. Lee, A. Neiman, and S. Kim, Coherence resonance in a Hodgkin-Huxley neuron, Phys. Rev. E **57**, 3292 (1998).

[8] Y.-Q. Wang, David T. W. Chik, and Z. D. Wang, Coherence resonance and noise-induced synchronization in globally coupled Hodgkin-Huxley neurons, Phys. Rev. E **61**, 740 (2000).

[9] C. Zhou and J. Kurths, Noise-induced synchronization and coherence resonance of a Hodgkin-Huxley model of thermally sensitive neurons, Chaos **13**, 401 (2003).

[10] L. A. da Silva and R. D. Vilela, Colored noise and memory effects on formal spiking neuron models, Phys. Rev. E **91**, 062702 (2015).

[11] E. Yilmaza, V. Baysala, and M. Ozer, Enhancement of temporal coherence via time-periodic coupling strength in a scale-free network of stochastic Hodgkin-Huxley neurons, Phys. Lett. A **379**, 1594 (2015).

[12] X.-M. Guo, J. Wang, J. Liu, H.-T. Yu, and R. F. Galán, Optimal time scales of input fluctuations for spiking coherence and reliability in stochastic Hodgkin-Huxley neurons, Physica A **468**, 381 (2017).

[13] H.-T. Yu, R. F. Galán, J. Wanga, Y.-B. Cao, and J. Liu, Stochastic resonance, coherence resonance, and spike timing reliability of Hodgkin-Huxley neurons with ion-channel noise, Physica A **471**, 263 (2017).

[14] Y.-H. Hao, Y.-B. Gong, X. Lin, Y.-H. Xie, and X.-G. Ma, Transition and enhancement of synchronization by time delays in stochastic Hodgkin-Huxley neuron networks, Neurocomputing, **73**, 2998 (2010).

[15] R. Kubo, Statistical-mechanical theory of irreversible processes. I. General theory and simple applications to magnetic and conduction problems, J. Phys. Soc. Jpn. **12**, 570 (1957).

[16] L. O. Chua, Memristor-The missing circuit element, IEEE Trans. Circuit Theory **18**, 507 (1971).

[17] L. O. Chua and S. M. Kang, Memristive devices and systems, Proc. IEEE **64**, 209 (1976).

[18] J. Biamonte, P. Wittek, N. Pancotti, P. Rebentrost, N. Wiebe, and S. Lloyd, Quantum Machine Learning, Nature **549**, 195 (2017).

[19] M. Mohseni, P. Rebentrost, S. Lloyd, and A. Aspuru-Guzik, Environment-assisted quantum walks in photosynthetic energy transfer, J. Chem. Phys. **129**, 174106 (2008).

[20] M. Mohseni, Y. Omar, G. S. Engel, and M. B. Plenio, *Quantum effects in biology* (Cambridge University Press, Cambridge, 2014).

[21] U. Alvarez-Rodriguez, M. Sanz, L. Lamata, and E. Solano, Artificial Life in Quantum Technologies, Sci. Rep. **6**, 20956 (2016).

[22] U. Alvarez-Rodriguez, M. Sanz, L. Lamata, and E. Solano, Quantum Artificial Life in an IBM Quantum Computer, Sci. Rep. **8** 14793 (2018).

[23] U. Alvarez-Rodriguez, M. Sanz, L. Lamata, and E. Solano, Biomimetic Cloning of Quantum Observables, Sci. Rep. **4**, 4910 (2014).

[24] P. Pfeiffer, I. L. Egusquiza, M. Di Ventra, M. Sanz, and E. Solano, Quantum Memristor, Sci. Rep. **6**, 29507 (2016).

[25] J. Salmilehto, F. Deppe, M. Di Ventra, M. Sanz, and E. Solano, Quantum Memristors with Superconducting Circuits, Sci. Rep. **7**, 42044 (2017).

[26] M. Sanz, L. Lamata, and E. Solano, Quantum Memristors in Quantum Photonics, APL Photonics **3**, 080801 (2018).

[27] D. Yu, H. H.-C. Iu, Y. Liang, T. Fernando, and L. O. Chua, Dynamic Behavior of Coupled Memristor Circuits, IEEE Trans. Circuits and Systems I **62**, 1607 (2015).

[28] R. K. Budhathoki, M. Pd. Sah, S. P. Adhikari, H. Kim, and L. O. Chua, Composite Behavior of Multiple Memristor Circuits, IEEE Trans. Circuits and Systems I **60**, 2688 (2013).

[29] L. O. Chua, Resistance Switching Memories are Memristors, Applied Physics A **102**, 765 (2011).

[30] G. Alvarado Barrios, J. C. Retamal, E. Solano, and M. Sanz, "Analog simulator of integro-differential equations with classical memristors", arXiv: 1803.05945 (2018).

[31] N. Gomez, J. O. Winter, F. Shieh, A. E. Saunders, B. A. Korgel, and C. E. Schmidt, Challenges in quantum dot-neuron active interfacing, Talanta, **67**, 462 (2005).

[32] M. Maeda, M. Suenaga, and H. Miyajima, Qubit neuron according to quantum circuit for XOR problem, Appl. Math. Comput. **185**, 1015 (2007).

[33] Michail Zak, From quantum entanglement to mirror neuron, Chaos, **34**, 344 (2007).

[34] D. Ventura and T. Martinez, *An Artificial Neuron with Quantum Mechanical Properties* (Springer, Vienna, 1998), pp. 482-485.

[35] Y. Cao, G. G. Guerreschi, and A. Aspuru-Guzik, Quantum Neuron: an elementary building block for machine learning on quantum computers, arXiv: 1711.11240

(2017).
[36] N. Kouda, N. Matsui, and H. Nishimura, Learning performance of neuron model based on quantum superposition, IEEE RO-MAN, 112 (2000).
[37] E. Prati, Quantum neuromorphic hardware for quantum artificial intelligence, J. Phys.: Conf. Ser. **880**, 012018, (2017).
[38] G. S. Snider *et al.*, From synapses to circuitry: Using memristive memory to explore the electronic brain, Computer **44**, 21 (2011).
[39] R. Berdan, E. Vasilaki, A. Khiat, G. Indiveri, A. Serb, and T. Prodromakis, Emulating short-term synaptic-dynamics with memristive devices, Sci. Rep. **6**, 18639 (2015).
[40] Y. V. Pershin and M. Di Ventra, Neuromorphic, Digital, and Quantum Computation with Memory Circuit Elements, Proc. IEEE **100**, 2071 (2012).
[41] T. Serrano-Gotarredona, T. Masquelier, T. Prodromakis, G. Indiveri, and B. Linares-Barranco, STDP and STDP variations with memristors for spiking neuromorphic learning systems, Front. Neurosci. **7**, 2 (2013).
[42] T. Gonzalez-Raya, Master Thesis: *Quantized Hodgkin-Huxley Model for Quantum Neurons*, (Universidad del Pais Vasco, 2018).
[43] F. Silva, M. Sanz, J. Seixas, E. Solano, and Y. Omar, Perceptrons from Memristors, arXiv: 1807.04912 (2018).
[44] M. Schuld, I. Sinayskiy, and F. Petruccione, An introduction to quantum machine learning, Contemp. Phys. **56**, 172 (2015).
[45] L. O. Chua, V. Sbitnev, and H. Kim, Hodgkin-Huxley axon is made of memristors, Int. J. Bifurcation Chaos **22**, 1230011 (2012).
[46] G. Z. Cohen, Y. V. Pershin, and M. Di Ventra, Lagrange Formalism of Memory Circuit Elements: Classical and Quantum Formulation, Phys. Rev. B **85**, 165428 (2012).
[47] U. Vool and M. Devoret, Introduction to Quantum Electromagnetic Circuits, Int. J. Circuit Theory and Applications **45**, 897 (2016).
[48] B. Yurke and J. S. Denker, Quantum Network Theory, Phys. Rev. A **29**, 1419 (1984).
[49] M. Sanz, E. Solano, and I. L. Egusquiza, *Beyond Adiabatic Elimination: Effective Hamiltonians and Singular Perturbation* (Springer, Japan, 2016), pp. 127-142.
[50] S. Peotta and M. Di Ventra, Superconducting Memristors, Phys. Rev. Appl. **2**, 034011 (2014).
[51] T. Gonzalez-Raya, E. Solano, and M. Sanz, Quantized Three-Ion-Channel Model for Neural Action Potentials, arXiv: 1906.07570 (2019).